Chemical Engineering Journal 471 (2023) 144552

Contents lists available at ScienceDirect

Chemical Engineering Journal

journal homepage: www.elsevier.com/locate/cej

# Isovalent multi-component doping strategy for stabilizing cubic-$Li_7La_3Zr_2O_{12}$ with excellent Li mobility

Han Uk Lee [a,b], Seungmin Han [c,d], Dong Geon Lee [e,g], Hyunseok Ko [e], Juhyun Lee [c,f], Won Bin Im [g], Taeseup Song [d], Junghyun Choi [c,*], Sung Beom Cho [a,b,*]

[a] Department of Materials Science and Engineering, Ajou University, Suwon, Gyeonggi-do 16499, Republic of Korea
[b] Department of Energy Systems Research, Ajou University, Suwon 16499, Republic of Korea
[c] Energy Storage Materials Center, Korea Institute of Ceramic Engineering and Technology (KICET), Jinju, Gyeongsangnam-do 52851, Republic of Korea
[d] Department of Energy Engineering, Hanyang University, Seoul 04763, South Korea
[e] Center of Materials Digitalization, Korea Institute of Ceramic Engineering and Technology (KICET), Jinju, Gyeongsangnam-do 52851, Republic of Korea
[f] Department of Materials Science and Engineering, Pusan National University, Busan 46241, South Korea
[g] Division of Materials Science and Engineering, Hanyang University, Seoul 04763, South Korea

ARTICLE INFO

*Keywords:*
All-solid-state battery
Solid-state electrolyte
$Li_7La_3Zr_2O_{12}$
Multi-component alloy
Reduction sintering temperature

ABSTRACT

Stabilizing the cubic phase of $Li_7La_3Zr_2O_{12}$ (LLZO) through doping has been a challenging issue, as conventional aliovalent dopants often decrease Li ion mobility and induce unwanted phase transformations. In this study, a novel multi-component doping strategy is proposed that stabilizes the cubic phase of LLZO while maintaining high Li ion mobility. The practical isovalent ions and their combinations are screened using density-functional theory (DFT) calculations and ab-initio molecular dynamics (AIMD) simulations, identifying the most stable multi-component alloy configuration that can stabilize the robust cubic phase of LLZO. Our results demonstrate that the proposed $Li_7La_3(Zr, Hf, Ce, Ru)_2O_{12}$ composition has a stable cubic phase at low temperatures, which we validated through experimental synthesis. Our proposed doping strategy has the potential to advance the development of high-performance all-solid-state batteries.

## 1. Introduction

With a widespread transition of energy storage technologies from portable electric vehicles to energy-grid, advanced battery technologies are required to overcome the conventional Li-ion battery issues, such as low energy density, narrow operable temperature, and poor safety [1–3]. In this scenario, all-solid-state battery systems are emerging as a game changer to outperform traditional battery systems in the three aspects of merit: energy density, operable temperature, and safety [4,5]. Among them, garnet-based $Li_7La_3Zr_2O_{12}$ (LLZO) materials are promising candidates for replacing traditional liquid-state electrolytes, due to their high ionic conductivity, high chemical stability against to Li, and a wide electrochemical window compared with other solid-state electrolyte such as LIPON, NASICON, and perovskites [4,6–8].

Despite the fascinating properties of LLZO as a solid-state electrolyte, there are still challenges in achieving high ionic conductivity at room temperature. The ground state of LLZO is a tetragonal structure that exhibits poor Li ion conductivity lower by two orders of magnitude than that cubic structure [9–11]. In principle, cubic structure can be stabilized above 650℃ by increasing the configuration entropy of Li-ion [9,12]. However, this transition is thermodynamically reversible and involves complex mechanism [13], so that the practical control of single phase is difficult at that temperature. The phase transition from cubic to tetragonal is also observed in the cooling process after the solid-state reaction [13]. In addition, the instability of the cubic phase also leads to undesirable phase transformation from cubic to tetragonal during battery operation.

Since the phase transformation is triggered by Li vacancy concentration [14], the most common approach to attain the cubic phase is by introducing Li vacancy with aliovalent cations. When the aliovalent cations substitute the cation sites of LLZO, the Li vacancies are created to maintain the charge balance. For the purpose, the Al/Ga doping for Li sites or Nb/Ta doping for Zr sites are commonly used, but both of doping strategy have limitations. The super valent cations ($Al^{3+}$ and $Ga^{3+}$) into

* Corresponding authors at: Energy Storage Materials Center, Korea Institute of Ceramic Engineering and Technology (KICET), Jinju, Gyeongsangnam-do 52851, Republic of Korea (J. Choi). Department of Materials Science and Engineering, Ajou University, Suwon, Gyeonggi-do 16499, Republic of Korea (S.B. Cho).
*E-mail addresses:* jchoi@kicet.re.kr (J. Choi), csb@ajou.ac.kr (S.B. Cho).

https://doi.org/10.1016/j.cej.2023.144552
Received 11 April 2023; Received in revised form 8 June 2023; Accepted 30 June 2023
Available online 1 July 2023

$Li^+$ sites generate a disorder of Li and vacant sites, resulting in the stabilization of cubic LLZO at room temperature [15,16]. However, this raises the undesirable issue of an Li mobility decrease because the occupancy of dopant in the Li sites blocks the Li diffusion path [17]. The other doping strategy, aliovalent ($Ta^{5+}$ or $Nb^{5+}$) doping into the $Zr^{4+}$ sites, also enhance the Li ion conductivity by forming Li vacancy as well [18,19]. However, this substitutive doping leads Li site preference and vacancy ordering, resulting cubic-to-tetragonal phase transition [9]. Therefore, it is still necessary to develop more efficient doping strategy which can increase both stability of cubic phase and ionic conductivity.

In this work, we investigated the phase stability of LLZO-based multi-component alloy systems using density-functional theory (DFT) and performed ab-initio molecular dynamics (AIMD) simulations. To address the doping issue between phase stability and Li ion mobility, we investigated a rational multi-component dopant strategy. We selected seven isovalent elements in the periodic table to maintain Li stoichiometry and generated 35 configurations of multi-component alloy. We identified a way to robustly stabilize the cubic phase by calculating the enthalpy of mixing for all the candidates. To investigate phase competition as a function of temperature, we calculated the Gibbs free energies and found the $Li_7La_3(Zr, Hf, Ce, Ru)_2O_{12}$ that can be stable at the lowest temperature among them. We confirmed that the multi-component system stabilized the cubic-phase and sufficiently decreased the synthesis temperature in the solid-state reaction. Finally, we performed AIMD calculation for $Li_7La_3(Zr, Hf, Ce, Ru)_2O_{12}$ to estimate the Li diffusion performance of solid electrolytes and obtained higher Li-diffusion coefficient than pure cubic-LLZO.

## 2. Method

***DFT calculations***: We modeled all multi-component alloy systems based on LLZO by special quasi-random structures (SQS) [20], by using the *mcsqs* code provided in the alloy theoretic automated toolkit (ATAT) [21]. To satisfy the disordered criteria, all SQS were generated by considering the 3rd nearest neighbors. All density functional theory (DFT) was performed by using the Vienna ab-initio simulation package (VASP) [22]. The Perdew-Burke-Ernzerhof (PBE) fuctional was used to describe the exchange–correlation energy of valence electorns [23]. The valence states of each cation was selected as following: Li_sv (1s2s2p) for Li, La (5s5p5d6s) for La, Zr_sv (4s4p4d5s) for Zr, Hf_pv (5p5d6s) for Hf, Ce (4f5s5p5d6s) for Ce, Ru_pv (4p4d5s) for Ru, and O (s2p4) for O. The plane-wave cuttoff energy was set to 600 eV and the projector augmented method was utilized [24]. The structural optimization was truncated after the Hellmann-Feynman forces were under 0.001 $eV/Å$. The Brillouin zone was sampled using a 100 k-points density per $Å^{-3}$ in the reciprocal lattice.

***Molecule Dynamics***: In this study, all molecule dynamics was conducted at each temperature using ab-initio molecular dynamics (AIMD) in VASP package. The DFT-based force evaluations were non-spin-polarized. The cutoff energy was set to 400 eV for the computational, and the Brillouin zone was sampled with Γ-points. We employed a 2 fs timestep for a total time range of 15 ps, and NVT ensemble using a Nose-Hoover thermostat. The mean square displacement (MSD) and diffusion coefficient were extracted by using VASPKIT [25].

***Sample preparation***: The starting martials of $Li_2O$ (97%), $La_2O_3$ (99.9%), $ZrO_2$ (99%), $HfO_2$ (98%), $CeO_2$ (99.9%) and $RuO_2$(99.9%) were purchased from Sigma-Aldrich and were mixed at molar ratio of 7: 3: 2 in jar. For $Li_7La_3(Zr, Hf, Ce, Ru)_2O_{12}$, the molar ratio between Zr, Hf, Ce and Ru was controlled as 0.5 (same as $Li_7La_3Zr_{0.5}Hf_{0.5}Ce_{0.5}Ru_{0.5}O_{12}$). The 10 mol% excess Li of total Li amount was added. The precursors were planetary-milled ((Pulverisette-7 Premium Line, Fritsch) under 300 rpm for 2 h with 5 mm zirconia balls (to powder ratio of 4: 1). In the air condition, the mixed precursors were calcined in the box furnace at each temperature (600, 800 and 1000℃) for 12 h. The heating rate was 10 °C $min^{-1}$.

***X-ray Diffraction (XRD)***: XRD (D8 ADVANCE, BRUKER) was utilized to characterize the crystalline structure of synthesized solid electrolytes according to temperature at 600 °C – 1000 °C. XRD measurements of $Li_7La_3Zr_2O_{12}$ powders and $Li_7La_3(Zr, Hf, Ce, Ru)_2O_{12}$ powders were obtained in the 2θ range of 10 – 90° at a scan rate of 2.5° $min^{-1}$ using Cu-Kα radiation operating at 40 kV and 40 mA.

## 3. Result & discussion

Owing to the unique crystal structure and flexible chemical composition, garnet-based oxides have been widely used from expensive gemstones to functional materials for batteries [2,4], lasers [26], and biomedical usages [27]. The skeleton structure of garnet is constructed as $A_3B'_3B''_2O_{12}$, where the B″ cations occupy in the octant corners and center to form a body-centered cubic (bcc)-like structure in all other octants of a unit cell, and each octant face has an A-B′ unit whose arrangement is repeated, rotating by 180° compared with adjacent octants [28]. Inheriting the skeleton of the garnet, the $Li_7La_3Zr_2O_{12}$ is made up of (1) bcc-like $Zr^{4+}$ (B″) sublattice, (2) $La^{3+}$ (B′) sublattice, and (3) the decided skeleton that accommodates Li atoms in the interstitial sites generated by the B' and B" cations [29]. To occupy the optimized position in the unit cell, Li ions arrange via the coulombic interactions with adjacent Li-ions. This Li distribution rule based on the coulombic interaction plays a significant role in distinguishing the polymorphs of LLZO as a function of temperature [29,30].

In the ground state, the position of Li atoms is predominantly determined by reducing the coulomb repulsion between Li atoms. Consequently, the tetragonal phase prefers to have an ordered Li arrangement occupying the tetrahedral site (8a), octahedral site (16f), and the distorted octahedral site (32 g) as shown in Fig. 1(a) [29,30]. With an increase in temperature, the thermal energies provide a degree of freedom against the coulomb repulsion between adjacent Li ions. As a result, the Li arrangement becomes random in high temperatures, driving the phase transformation from the tetragonal to the cubic phase above 650°C [9,10]. In the disordered state, the Li randomly distributes on the tetrahedral site (24d), and the distorted octahedral site (96 h), as shown in Fig. 1(b) [29]. Despite the configurational immensity of possible Li configurations, we can generate the cubic structure following the electrostatic rule. The detailed method for cubic-LLZO atomic structure is described in the Supplementary material.

Based on the well-established atomic structure of the tetragonal and cubic, the Zr site is a favorable host cation site to obtain a successful muti-component alloy. We took a hint from the well-known fact that successful multi-component oxides can be achieved based on highly symmetric crystals, such as cubic and hexagonal structures [31–33]. Therefore, we suggest that the Zr site, which constructs the bcc-like sublattice in LLZO, could be a tailored host for mixing multiple cations. We then screened the compatible cations with the same oxidation state from the periodic table, as shown in Fig. 2. Elements such as noble metals, actinides, and those that easily form anions were excluded. Toxic, radioactive, and expensive elements were also filtered out. The remaining elements were classified based on their defect formation energies to determine whether they could be suitable substitutions on the Zr site, according to a pervious report about single element doping [34]. To validate the impact of mixing multiple cations, we fixed the Li stoichiometry by avoiding aliovalent elements. Finally, we identified seven candidates namely $Ti^{4+}$, $Mo^{4+}$, $Ru^{4+}$, $Sn^{4+}$, $W^{4+}$, $Ce^{4+}$, $Hf^{4+}$, and $W^{4+}$. To obtain a suitable SQS structure, we mixed three elements from a pool of seven candidates with Zr. Through a straightforward mathematical combination method, we generated 35 potential candidates.

The phase stability of the 35 alloy combinations was determined by DFT calculations combined with a regular solution model. By calculating the Gibbs free energy of mixing, we were able to infer whether alloy processes would be stable or unstable. This Gibbs free energy of mixing is defined as:

$$\Delta G_{mix}(T) = \Delta H_{mix} - T\Delta S_{tot} \quad (1)$$

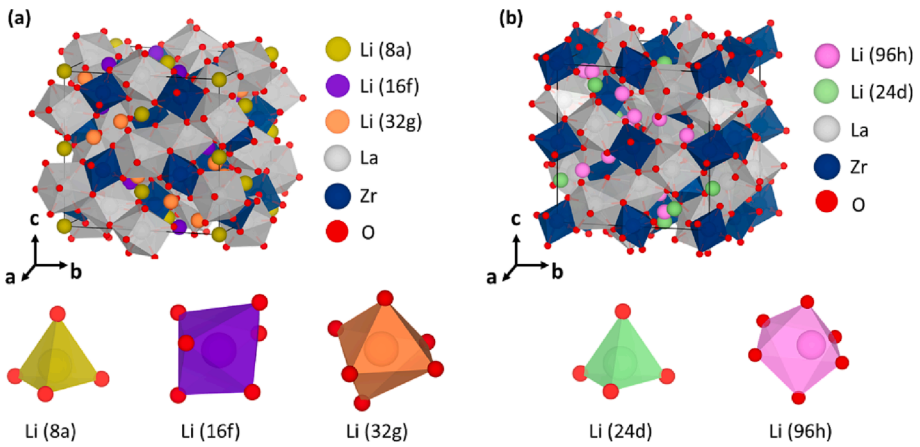


**Fig 1.** Polymorphs of LLZO. (a) tetragonal, and (b) cubic phase. The interstitial of Li ions named following Wyckoff notation.

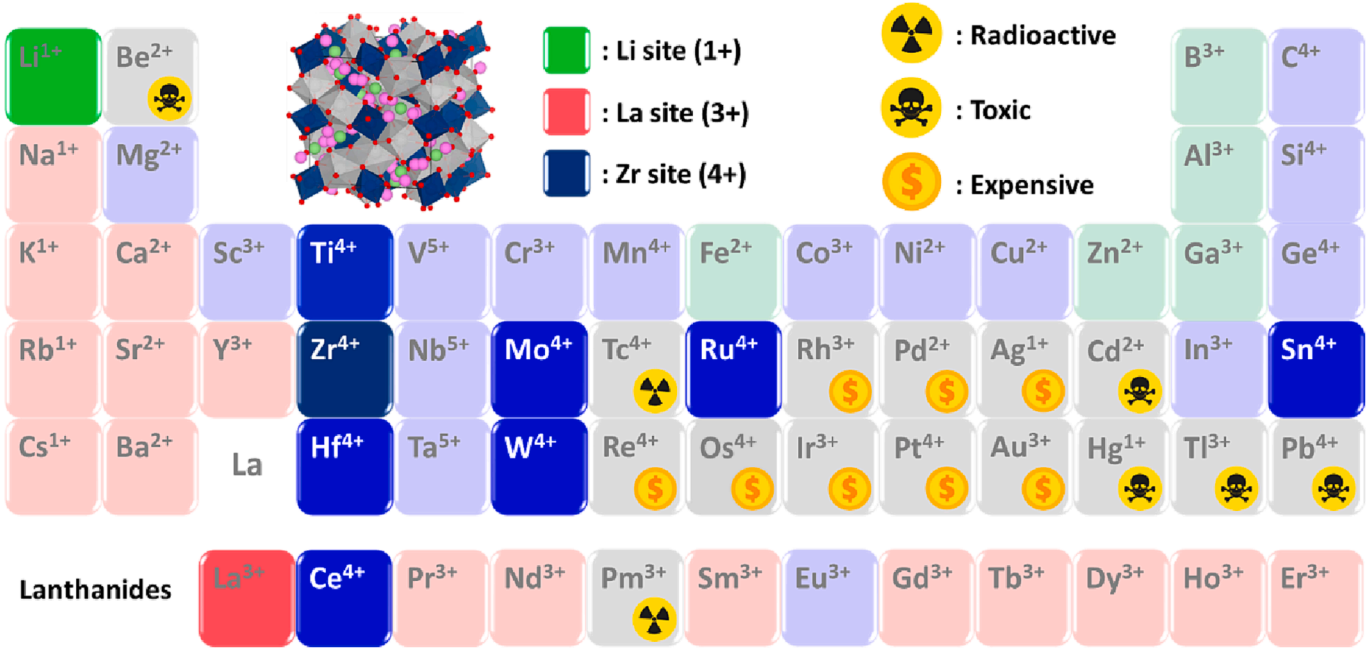


**Fig 2.** The possible dopant for multi-component alloy on Zr site. The green, red, and blue indicate compatible element with Li, La, and Zr, respectively. The grey is incompatible elements for alloy. (For interpretation of the references to colour in this figure legend, the reader is referred to the web version of this article.)

where $\Delta H_{mix}$ is the enthalpy of mixing, $T$ is the temperature, and $\Delta S_{tot}$ is the total entropy. The enthalpy of mixing is estimated by considering the interaction energy of each constituent cation in binary oxide systems and is defined as:

$$\Delta H_{mix}\left[Li_7La_3\left(\begin{matrix}Zr,A,\\B,C\end{matrix}\right)_2O_{12}\right] = E_{DFT}\left[Li_7La_3\left(\begin{matrix}Zr,A,\\B,C\end{matrix}\right)_2O_{12}\right] - x \times \sum E_{DFT}\left[X_yO_z\right] \quad (2)$$

where $E_{DFT}\left[Li_7La_3(Zr,A,B,C)_2O_{12}\right]$ is the total energy of the crystal structure of the random alloy, $x$ is the molar concentration, and $E_{DFT}\left[X_xO_y\right]$ are the total energies of the binary oxide of each cation. We selected binary oxides with the same ionic valence as the multi-component alloy for the constituent cations, such as $Li_2O$, $La_2O_3$, $ZrO_2$, $HfO_2$, $CeO_2$, $MoO_2$, $WO_2$, $SnO_2$, and $RuO_2$.

It is interesting to note that none of the configurations have $\Delta H_{mix} > 0$, which represents a thermodynamically unstable region as shown in Fig S2. This indicates that all the alloy processes of both polymorphs are thermodynamically stable. Hence, to evaluate the phase competition between the tetragonal and cubic, we investigated the $\Delta H_{cubic-tetragonal}$, as shown in Fig. 3a. Unfortunately, the tetragonal phase was found to be more stable than cubic phase, meaning that $\Delta H_{cubic-tetragonal} > 0$. However, some candidates showed the potential to achieve a low transition temperature, resulting from a smaller $\Delta H_{cubic-tetragonal}$ than pure LLZO (0.07 eV, our calculation result). We then considered the total entropy for multi-component alloy systems based on LLZO to evaluate the Gibbs free energies of mixing. The detailed method of total entropy calculation is described in the Supplementary material.

We calculated the Gibbs free energies of mixing for all the configurations as a function of the temperature. The difference in Gibbs free energy ($\Delta G_{cubic-tetragonal}$) was used to evaluate the phase competition between polymorphs, as shown in Fig. 3b. The thermodynamic boundary of phase competition, where $\Delta G_{cubic-tetragonal} = 0$, represents the equilibrium state between the tetragonal and cubic phase. The tetragonal phase is stable at $\Delta G_{cubic-tetragonal} > 0$, *vice versa* the cubic phase is stable at $\Delta G_{cubic-tetragonal} < 0$. Interestingly, the Gibbs free energies show that several cubic phases win the phase competition against the

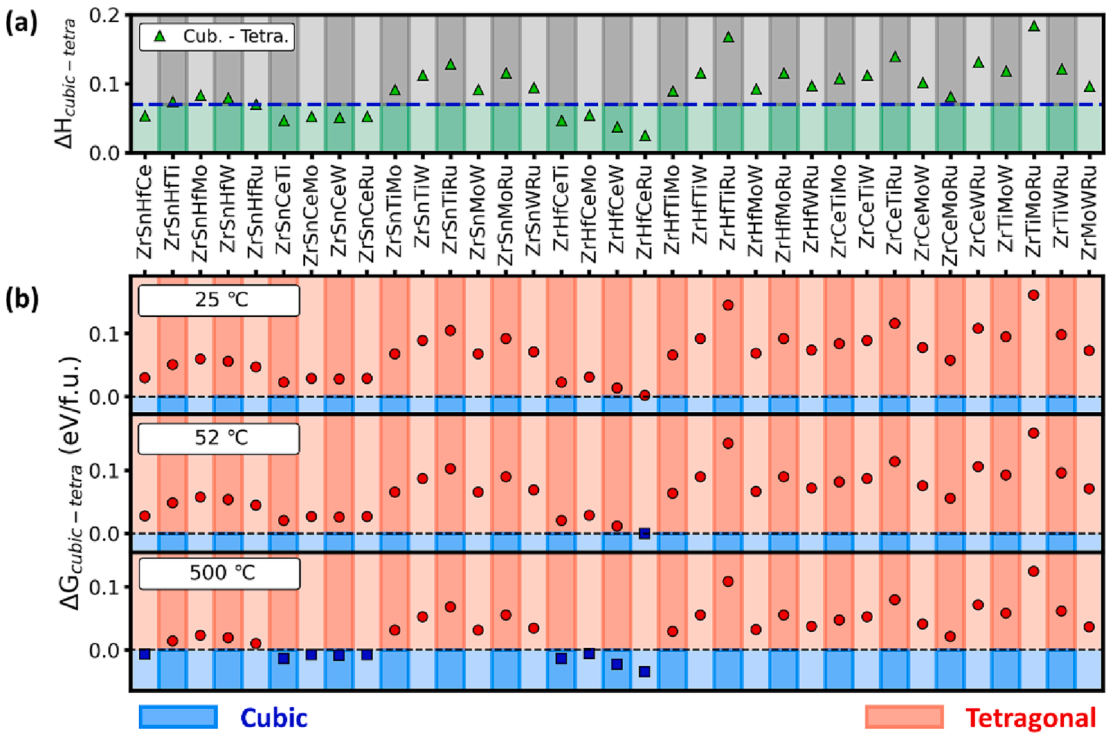


**Fig 3.** (a) The difference of enthalpies of mixing between the tetragonal and cubic LLZO-based alloy. The blue dashed line represents the energy difference between tetragonal and cubic for pure-LLZO (0.07 eV). The green shadow region indicates the smaller energy difference compared with pure-LLZO. (b) Gibbs free energy differences for LLZO-based multi-component alloy as a funtion of temperature. The black dashed lines represent the zero value of Gibbs free energy. The red, and blue colors indicate the thermodynamically stable state of the tetragonal and cubic respectively.

tetragonal phases as the temperature increase. Notably, $Li_7La_3$(Zr, Hf, Ce, Ru)$_2O_{12}$ was identified as a promising candidate because it has drastically reduced its transition temperature (52℃) compared to pure LLZO (650 ~ 700℃). This result suggests that multi-component LLZO alloys can be an effective way to provide a significant driving force for cubic-phase synthesis at low temperatures and its stabilization.

To verify the calculation results, we investigated the phase stability of $Li_7La_3Zr_2O_{12}$ and $Li_7La_3$(Zr, Hf, Ce, Ru)$_2O_{12}$ synthesized by solid-state reaction. The XRD patterns for the $Li_7La_3Zr_2O_{12}$ and $Li_7La_3$(Zr, Hf, Ce, Ru)$_2O_{12}$ are obtained in room temperature after the 1000 , 800 and 600 ℃ calcination, as shown in Fig. 4. As represented in Fig. 4a, the diffraction peaks of (211)/(112) and (220)/(202) indicated that the pure LLZO has a tetragonal phase with the $I\,4_1/acd$ space group. On the other hand, the XRD pattern of cubic phase with the $Ia\,\bar{3}\,d$ space group was observed by (211) and (220) peaks of $Li_7La_3$(Zr, Hf, Ce, Ru)$_2O_{12}$. The formation of cubic phase implies that the substitution with dopants for Zr sites is successfully achieved. The X-ray Photoelectron Spectroscopy (XPS) analysis results were also supported to demonstrate substitution of dopants for Zr sites, as shown in Fig. S3. In the Zr 3d spectra of $Li_7La_3$(Zr, Hf, Ce, Ru)$_2O_{12}$, the decreased $Zr^{4+}$ signal was observed compared to $Li_7La_3Zr_2O_{12}$. It is attributed to reduce the content of Zr by introducing other dopants. Besides the new peaks were emerged in the Hf 4f, Ce 3d and Ru 3p spectra, which is inferred that each dopant is doped into cubic phase while maintaining the 4 + oxidation state. These results corroborate that the dopants were properly substituted for $Zr^{4+}$. Also, the cubic phase of $Li_7La_3$(Zr, Hf, Ce, Ru)$_2O_{12}$ was identified at low temperature as shown in Fig. 4c. It indicates that the dopants composing $Li_7La_3$(Zr, Hf, Ce, Ru)$_2O_{12}$ effectively stabilize the cubic phase, enabling low-temperature synthesis. This stabilized cubic phase of the $Li_7La_3$(Zr, Hf, Ce, Ru)$_2O_{12}$ can induce a higher ionic conductivity compared to that of pure LLZO due to its improved lithium ions diffusion pathway [35].

We believe that the remarkable stability of the cubic phase is a result of synergetic effects among the multiple cations. Zr, Hf, Ce, and Ru are well-known to possess stable 4 + oxidation states [36], and they are in the same groups except for Ru. Crystallography-wise, these cations are well satisfied with the cation-to-oxygen ratio between 0.4 and 0.6, which prefer to generate 6-fold coordination from Pauling's rule [28,36], as shown in Table S1. Further prove is the existence of $Li_7La_3Hf_2O_{12}$, where perfectly substitutes Hf for Zr [37]. There is also successful experimental report of Ru alloying in the Zr site that exhibits higher ion conductivity than pure LLZO [38]. In particular, it is assumed that Ce imparts robust cubic phase stability to $Li_7La_3$(Zr, Hf, Ce, Ru)$_2O_{12}$. The R. Djenadic et al. [39] showed that the phase stability is distinctly different for the samples include $Ce^{4+}$ and successful multi-component alloys which favor 4 + cations include Ce or Zr or both [39–41]. Furthermore, the Ce-doped LLZO can achieve low transition temperatures [42,43]. However, the phase stability mechanism for the multi-component alloy is difficult to predict accurately due to the complex synergies among the constituents, and it will be our further research.

Along with studying the phase stability of $Li_7La_3$(Zr, Hf, Ce, Ru)$_2O_{12}$, we also investigated the Li diffusion performance as a solid-state electrolyte. We performed an AIMD calculation to predict the Li diffusion performance and extracted the mean square displacements (MSDs), as shown in Fig. 5 (left). The figure shows that the Li diffusion is predominant already at 300 K, compared with other species. Using this MSDs, we predicted the diffusion coefficient of Li, as shown in Fig. 5 (right). According to this estimation, the Li diffusion coefficient of $Li_7La_3$(Zr, Hf, Ce, Ru)$_2O_{12}$ can be lower as five orders of magnitude higher than pure LLZO at 300 K. We estimate that the large Li diffusivity results from the lower activation barrier caused by the local structure change around Li ions [44]. Furthermore, the multi-component alloy can induce extensive local structure change resulting in a disordered environment around Li ions. These local distortions create the site-energy overlapping, which decrease activation energy for Li hoping and leads to an increase in the ion hopping network [35]. Since the diffusivity is inversely proportional to the exponential of the activation barrier, the improved Li diffusion coefficient results from the low

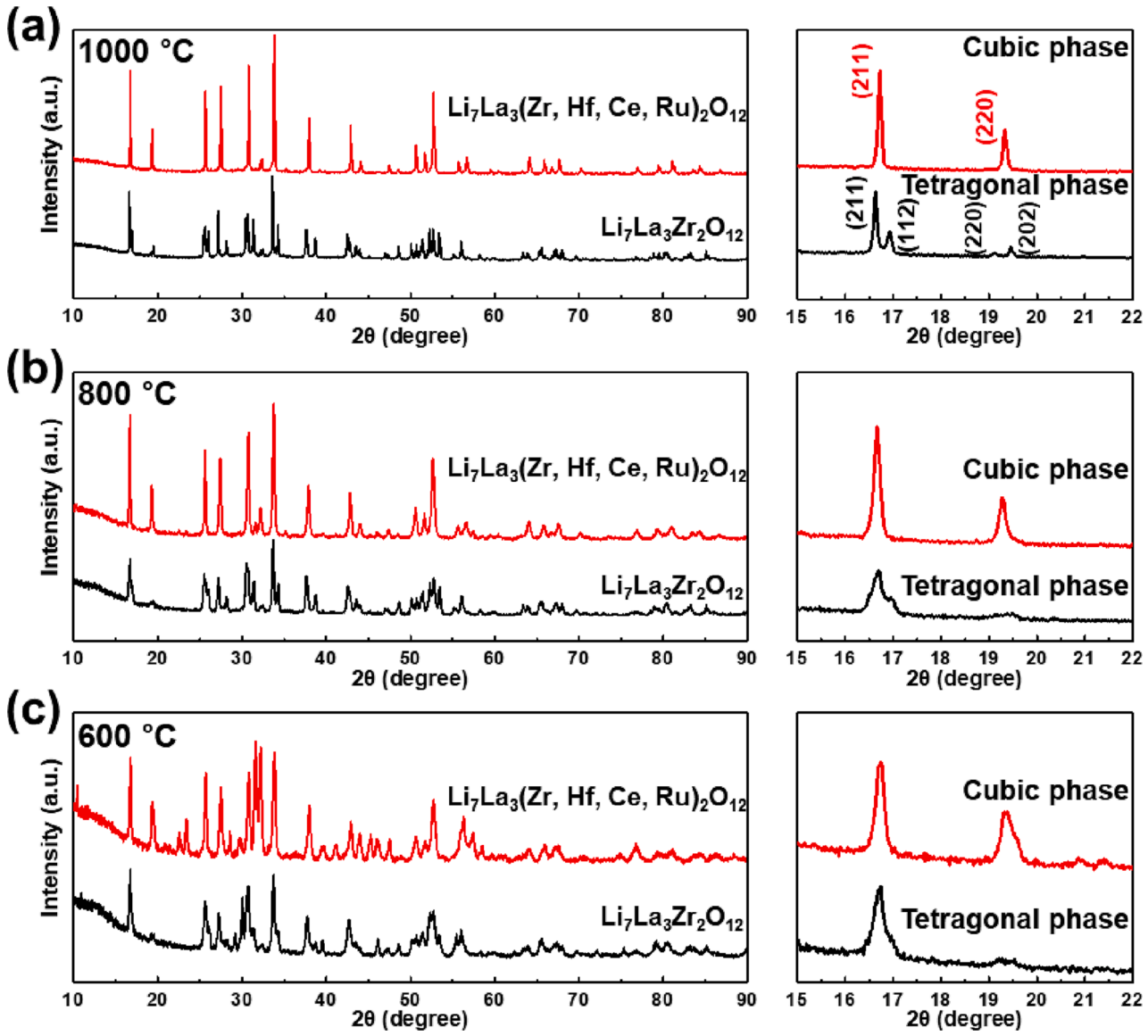


**Fig 4.** (a) X-ray diffraction patterns of $Li_7La_3Zr_2O_{12}$ and $Li_7La_3(Zr, Hf, Ce, Ru)_2O_{12}$ calcinated at 1000 ℃, (b) 800 ℃ and (c) 600 ℃.

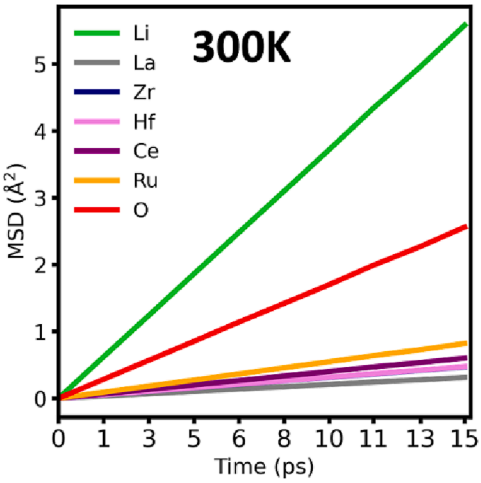


| Temperature [K] | Li diffusion coefficient [cm²/s] | |
|---|---|---|
| | Pure LLZO | LL(Zr, Hf, Ce, Ru)O |
| 300 | $1.69 * 10^{-11}$ | $0.67 * 10^{-6}$ |
| 500 | $1.34 * 10^{-7}$ | $0.14 * 10^{-4}$ |
| 700 | $6.72 * 10^{-6}$ | $0.16 * 10^{-4}$ |
| 900 | $1.43 * 10^{-5}$ | $0.21 * 10^{-4}$ |

**Fig 5.** The mean square displacement (MSD) of all ions, at 300 K (left). The table represent the Li diffusion coefficient of $Li_7La_3(Zr, Hf, Ce, Ru)_2O_{12}$ compared with pure LLZO, at each temperature. The Li diffusion coefficient value of pure LLZO was extracted from Stephen R. Yeandel et al. [45].

activation energy induced by multi-component alloy.

Despite several reported doping strategies, trade-off relationship between Li ion conductivity and cubic phase stabilization in LLZO has yet to be fully resolved. Our calculations exhibit that $Li_7La_3$(Zr, Hf, Ce, Ru)$_2O_{12}$ composition not only exhibits high cubic phase stability but also possesses great Li ion conductivity. The combination of enhanced Li-ion conductivity and high structural stability makes room temperature operation feasible. We believe that this possibility for room temperature operation will significantly broaden the potential application field of all-solid-state batteries.

## 4. Conclusion

In this study, we investigated the phase stability of cubic-LLZO using isovalent multi-component doping approach. Our analysis showed that the multicomponent approach is an effective way to stabilize the cubic phase, as demonstrated by calculated thermodynamic properties for various multi-component doping configurations. Specifically, we found that doping the Zr site with Hf, Ce, and Ru can significantly reduce the sintering temperature and stabilize the cubic phase. We validated this multi-component doping approach through solid-state reaction and observed that the sample maintained its cubic structure at room temperature and under a sintering temperature of 600 ℃. Moreover, due to its hopping nature, we anticipate higher Li ionic diffusivity for this sample. Our results demonstrate the potential of the multicomponent doping strategy for achieving low-temperature sintering and highlight its practical applications in solid-state batteries.

## Declaration of Competing Interest

The authors declare that they have no known competing financial interests or personal relationships that could have appeared to influence the work reported in this paper.

## Data availability

Data will be made available on request.

## Acknowledgement

This research was supported by National R&D Program through the National Research Foundation of Korea (NRF) funded by Ministry of Science and ICT (2021M3C1C3097516, and RS-2023-00209910). The computational resource was partially supported by National Supercomputing Center (KSC-2022-CRE-0352).

## Appendix A. Supplementary data

Supplementary data to this article can be found online at https://doi.org/10.1016/j.cej.2023.144552.

## References

[1] Y. Tian, G. Zeng, A. Rutt, T. Shi, H. Kim, J. Wang, J. Koettgen, Y. Sun, B. Ouyang, T. Chen, Z. Lun, Z. Rong, K. Persson, G. Ceder, Promises and Challenges of Next-Generation "Beyond Li-ion" Batteries for Electric Vehicles and Grid Decarbonization, Chem. Rev. 121 (2021) 1623–1669, https://doi.org/10.1021/acs.chemrev.0c00767.

[2] C. Wang, K. Fu, S.P. Kammampata, D.W. McOwen, A.J. Samson, L. Zhang, G. T. Hitz, A.M. Nolan, E.D. Wachsman, Y. Mo, V. Thangadurai, L. Hu, Garnet-Type Solid-State Electrolytes: Materials, Interfaces, and Batteries, Chem. Rev. 120 (2020) 4257–4300, https://doi.org/10.1021/acs.chemrev.9b00427.

[3] S. Rana, R. Kumar, R.S. Bharj, Current trends, challenges, and prospects in material advances for improving the overall safety of lithium-ion battery pack, Chem. Eng. J. 463 (2023), 142336, https://doi.org/10.1016/j.cej.2023.142336.

[4] L. Xu, J. Li, W. Deng, H. Shuai, S. Li, Z. Xu, J. Li, H. Hou, H. Peng, G. Zou, X. Ji, Garnet Solid Electrolyte for Advanced All-Solid-State Li Batteries, Adv. Energy Mater. 11 (2021) 2000648, https://doi.org/10.1002/aenm.202000648.

[5] J. Choi, P.J. Kim, A roadmap of battery separator development: Past and future, Curr. Opin. Electrochem. 31 (2022), 100858, https://doi.org/10.1016/j.coelec.2021.100858.

[6] T. Wu, W. Dai, M. Ke, Q. Huang, L. Lu, All-Solid-State Thin Film μ-Batteries for Microelectronics, Adv. Sci. 8 (2021) 2100774, https://doi.org/10.1002/advs.202100774.

[7] S. Kim, J.-S. Kim, L. Miara, Y. Wang, S.-K. Jung, S.Y. Park, Z. Song, H. Kim, M. Badding, J. Chang, V. Roev, G. Yoon, R. Kim, J.-H. Kim, K. Yoon, D. Im, K. Kang, High-energy and durable lithium metal batteries using garnet-type solid electrolytes with tailored lithium-metal compatibility, Nat. Commun. 13 (2022) 1883, https://doi.org/10.1038/s41467-022-29531-x.

[8] H. Sun, S. Kang, L. Cui, Prospects of LLZO type solid electrolyte: From material design to battery application, Chem. Eng. J. 454 (2023), 140375, https://doi.org/10.1016/j.cej.2022.140375.

[9] F. Chen, J. Li, Z. Huang, Y. Yang, Q. Shen, L. Zhang, Origin of the Phase Transition in Lithium Garnets, J. Phys. Chem. C 122 (2018) 1963–1972, https://doi.org/10.1021/acs.jpcc.7b10911.

[10] N. Bernstein, M.D. Johannes, K. Hoang, Origin of the Structural Phase Transition in $Li_7La_3Zr_2O_{12}$, Phys. Rev. Lett. 109 (2012), 205702, https://doi.org/10.1103/physrevlett.109.205702.

[11] C.A. Geiger, E. Alekseev, B. Lazic, M. Fisch, T. Armbruster, R. Langner, M. Fechtelkord, N. Kim, T. Pettke, W. Weppner, Crystal Chemistry and Stability of "$Li_7La_3Zr_2O_{12}$" Garnet: A Fast Lithium-Ion Conductor, Inorg. Chem. 50 (2011) 1089–1097, https://doi.org/10.1021/ic101914e.

[12] Y. Hu, T. Feng, L. Xu, L. Zhang, L. Luo, Probing the Phase Transition during the Formation of Lithium Lanthanum Zirconium Oxide Solid Electrolyte, Acs Appl Mater Inter. 14 (2022) 41978–41987, https://doi.org/10.1021/acsami.2c09660.

[13] A. Paolella, W. Zhu, G. Bertoni, S. Savoie, Z. Feng, H. Demers, V. Gariepy, G. Girard, E. Rivard, N. Delaporte, A. Guerfi, H. Lorrmann, C. George, K. Zaghib, Discovering the Influence of Lithium Loss on Garnet $Li_7La_3Zr_2O_{12}$ Electrolyte Phase Stability, Acs Appl. Energy Mater. 3 (2020) 3415–3424, https://doi.org/10.1021/acsaem.9b02401.

[14] N. Bernstein, M.D. Johannes, K. Hoang, Origin of the Structural Phase Transition in $Li_7La_3Zr_2O_{12}$, Phys. Rev. Lett. 109 (2012), 205702, https://doi.org/10.1103/physrevlett.109.205702.

[15] C. Chen, Y. Sun, L. He, M. Kotobuki, E. Hanc, Y. Chen, K. Zeng, L. Lu, Microstructural and Electrochemical Properties of Al- and Ga-Doped $Li_7La_3Zr_2O_{12}$ Garnet Solid Electrolytes, Acs Appl Energy Mater. 3 (2020) 4708–4719, https://doi.org/10.1021/acsaem.0c00347.

[16] R. Wagner, G.J. Redhammer, D. Rettenwander, A. Senyshyn, W. Schmidt, M. Wilkening, G. Amthauer, Crystal Structure of Garnet-Related Li-Ion Conductor $Li_{7-3x}$ $Ga_xLa_3Zr_2O_{12}$: Fast Li-Ion Conduction Caused by a Different Cubic Modification? Chem. Mater. 28 (2016) 1861–1871, https://doi.org/10.1021/acs.chemmater.6b00038.

[17] D.O. Shin, K. Oh, K.M. Kim, K.-Y. Park, B. Lee, Y.-G. Lee, K. Kang, Synergistic multi-doping effects on the $Li_7La_3Zr_2O_{12}$ solid electrolyte for fast lithium ion conduction, Sci. Rep.-Uk. 5 (2015) 18053, https://doi.org/10.1038/srep18053.

[18] T. Thompson, J. Wolfenstine, J.L. Allen, M. Johannes, A. Huq, I.N. David, J. Sakamoto, Tetragonal vs. cubic phase stability in Al – free Ta doped $Li_7La_3Zr_2O_{12}$ (LLZO), J. Mater. Chem. A 2 (2014) 13431–13436, https://doi.org/10.1039/c4ta02099e.

[19] K. Ishiguro, Y. Nakata, M. Matsui, I. Uechi, Y. Takeda, O. Yamamoto, N. Imanishi, Stability of Nb-Doped Cubic $Li_7La_3Zr_2O_{12}$ with Lithium Metal, J. Electrochem. Soc. 160 (2013) A1690–A1693, https://doi.org/10.1149/2.036310jes.

[20] A. Zunger, S.-H. Wei, L.G. Ferreira, J.E. Bernard, Special quasirandom structures, Phys. Rev. Lett. 65 (1990) 353–356, https://doi.org/10.1103/physrevlett.65.353.

[21] A. van de Walle, P. Tiwary, M. de Jong, D.L. Olmsted, M. Asta, A. Dick, D. Shin, Y. Wang, L.-Q. Chen, Z.-K. Liu, Efficient stochastic generation of special quasirandom structures, Calphad 42 (2013) 13–18, https://doi.org/10.1016/j.calphad.2013.06.006.

[22] G. Kresse, J. Furthmüller, Efficient iterative schemes for ab initio total-energy calculations using a plane-wave basis set, Phys. Rev. B 54 (1996) 11169–11186, https://doi.org/10.1103/physrevb.54.11169.

[23] J.P. Perdew, K. Burke, M. Ernzerhof, Generalized Gradient Approximation Made Simple, Phys. Rev. Lett. 77 (1996) 3865–3868, https://doi.org/10.1103/physrevlett.77.3865.

[24] P.E. Blöchl, Projector augmented-wave method, Phys. Rev. B 50 (1994) 17953–17979, https://doi.org/10.1103/physrevb.50.17953.

[25] V. Wang, N. Xu, J.-C. Liu, G. Tang, W.-T. Geng, VASPKIT: A user-friendly interface facilitating high-throughput computing and analysis using VASP code, Comput. Phys. Commun. 267 (2021), 108033, https://doi.org/10.1016/j.cpc.2021.108033.

[26] G. Liu, B. Wang, J. Li, B. Cao, Y. Lu, Z. Liu, Research progress of gadolinium aluminum garnet based optical materials, Phys. B Condens. Matter 603 (2021), 412775, https://doi.org/10.1016/j.physb.2020.412775.

[27] J. Xu, D. Murata, J. Ueda, S. Tanabe, Near-infrared long persistent luminescence of $Er^{3+}$ in garnet for the third bio-imaging window, J. Mater. Chem. C 4 (2016) 11096–11103, https://doi.org/10.1039/c6tc04027f.

[28] K.E. Sickafus, C.L. Melcher, M.I. Flynn-Hepford, Y. Wang, G. Jaroslaw, J.P. Smith, S.M. Drewry, M. Zhuravleva, Crystal chemistry of rare-earth containing garnets: Prospects for high configurational entropy, J. Solid State Chem. 310 (2022), 122997, https://doi.org/10.1016/j.jssc.2022.122997.

[29] J. Awaka, A. Takashima, K. Kataoka, N. Kijima, Y. Idemoto, J. Akimoto, Crystal Structure of Fast Lithium-ion-conducting Cubic $Li_7La_3Zr_2O_{12}$, Chem. Lett. 40 (2011) 60–62, https://doi.org/10.1246/cl.2011.60.

[30] J. Awaka, N. Kijima, H. Hayakawa, J. Akimoto, Synthesis and structure analysis of tetragonal $Li_7La_3Zr_2O_{12}$ with the garnet-related type structure, J. Solid State Chem. 182 (2009) 2046–2052, https://doi.org/10.1016/j.jssc.2009.05.020.
[31] C. Oses, C. Toher, S. Curtarolo, High-entropy ceramics, Nat. Rev. Mater. 5 (2020) 295–309, https://doi.org/10.1038/s41578-019-0170-8.
[32] S.-K. Jung, H. Gwon, H. Kim, G. Yoon, D. Shin, J. Hong, C. Jung, J.-S. Kim, Unlocking the hidden chemical space in cubic-phase garnet solid electrolyte for efficient quasi-all-solid-state lithium batteries, Nat. Commun. 13 (2022) 7638, https://doi.org/10.1038/s41467-022-35287-1.
[33] H. Xiang, Y. Xing, F. Dai, H. Wang, L. Su, L. Miao, G. Zhang, Y. Wang, X. Qi, L. Yao, H. Wang, B. Zhao, J. Li, Y. Zhou, High-entropy ceramics: Present status, challenges, and a look forward, J. Adv. Ceram. 10 (2021) 385–441, https://doi.org/10.1007/s40145-021-0477-y.
[34] L.J. Miara, W.D. Richards, Y.E. Wang, G. Ceder, First-Principles Studies on Cation Dopants and Electrolyte|Cathode Interphases for Lithium Garnetsx, Chem. Mater. 27 (2015) 4040–4047, https://doi.org/10.1021/acs.chemmater.5b01023.
[35] Y. Zeng, B. Ouyang, J. Liu, Y.-W. Byeon, Z. Cai, L.J. Miara, Y. Wang, G. Ceder, High-entropy mechanism to boost ionic conductivity, Science 378 (2022) 1320–1324, https://doi.org/10.1126/science.abq1346.
[36] Physical ceramics: principles for ceramic science and engineering, Choice Rev Online. 34 (1996) 34-1566-34–1566. 10.5860/choice.34-1566.
[37] J. Awaka, N. Kijima, K. Kataoka, H. Hayakawa, K. Ohshima, J. Akimoto, Neutron powder diffraction study of tetragonal Li7La3Hf2O12 with the garnet-related type structure, J. Solid State Chem. 183 (2010) 180–185, https://doi.org/10.1016/j.jssc.2009.10.030.
[38] B. Yan, M. Kotobuki, J. Liu, Ruthenium doped cubic-garnet structured solid electrolyte $Li_7La_3Zr_{2-x}Ru_xO_{12}$, Mater. Technol. 31 (2016) 623–627, https://doi.org/10.1080/10667857.2016.1196033.
[39] R. Djenadic, A. Sarkar, O. Clemens, C. Loho, M. Botros, V.S.K. Chakravadhanula, C. Kübel, S.S. Bhattacharya, A.S. Gandhi, H. Hahn, Multicomponent equiatomic rare earth oxides, Mater. Res. Letters. 5 (2017) 102–109, https://doi.org/10.1080/21663831.2016.1220433.
[40] M.R. Chellali, A. Sarkar, S.H. Nandam, S.S. Bhattacharya, B. Breitung, H. Hahn, L. Velasco, On the homogeneity of high entropy oxides: An investigation at the atomic scale, Scr. Mater. 166 (2019) 58–63, https://doi.org/10.1016/j.scriptamat.2019.02.039.
[41] J. Gild, M. Samiee, J.L. Braun, T. Harrington, H. Vega, P.E. Hopkins, K. Vecchio, J. Luo, High-entropy fluorite oxides, J. Eur. Ceram. Soc. 38 (2018) 3578–3584, https://doi.org/10.1016/j.jeurceramsoc.2018.04.010.
[42] B. Dong, S.R. Yeandel, P. Goddard, P.R. Slater, Combined Experimental and Computational Study of Ce-Doped $La_3Zr_2Li_7O_{12}$ Garnet Solid-State Electrolyte, Chem. Mater. 32 (2020) 215–223, https://doi.org/10.1021/acs.chemmater.9b03526.
[43] M.P. Stockham, A. Griffiths, B. Dong, P.R. Slater, Assessing the Importance of Cation Size in the Tetragonal-Cubic Phase Transition in Lithium-Garnet Electrolytes, Chem. – A Eur. J. 28 (2022) e202103442.
[44] K. Kang, G. Ceder, Factors that affect Li mobility in layered lithium transition metal oxides, Phys. Rev. B 74 (2006), 094105, https://doi.org/10.1103/physrevb.74.094105.
[45] S.R. Yeandel, B.J. Chapman, P.R. Slater, P. Goddard, Structure and Lithium-Ion Dynamics in Fluoride-Doped Cubic $Li_7La_3Zr_2O_{12}$ (LLZO) Garnet for Li Solid-State Battery Applications, J. Phys. Chem. C 122 (2018) 27811–27819, https://doi.org/10.1021/acs.jpcc.8b07704.